RSC Advances

ROYAL SOCIETY OF CHEMISTRY

www.rsc.org/advances

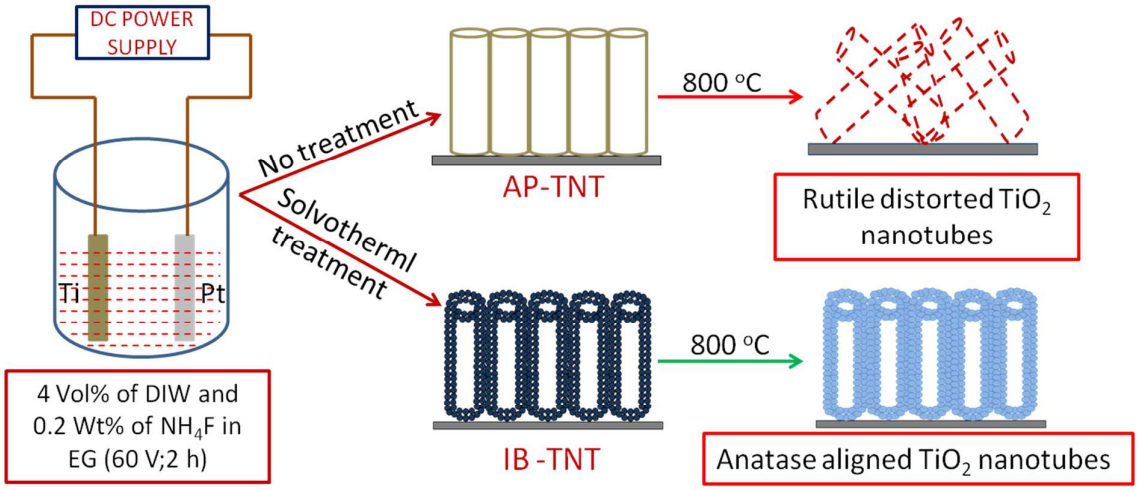

Solvothermal processing enhances the high temperature stability of the anatase phase and aligned morphology of electrochemically synthesized TiO_2 nanotube arrays

Anatase TiO_2 Nanotube Arrays with High Temperature Stability

B. Manmadha Rao and Somnath C. Roy #

Environmental Nanotechnology Laboratory, Department of Physics, Indian Institute of Technology Madras, Chennai 600036, India.

Corresponding author: somnath@iitm.ac.in

Abstract

The anatase phase of titanium dioxide (TiO_2) plays an important role in the applications such as photo-catalysis and photo-voltaics. The stability of this crystalline phase is however limited to about 600 ^oC because of the onset of anatase to rutile phase transformation. In the case of aligned and oriented nanostructures such as electrochemically anodized TiO_2 nanotube arrays (TNT), the retention of the aligned and oriented morphology, in addition to a stable anatase phase, poses further challenge for high temperature processing of such materials. Here we report a simple solvothermal processing step for the as-prepared, amorphous TNT that helps in retaining the nanotube architecture along with a stable anatase phase up to a temperature of about 800 ^oC. It is observed that the smoother walls of amorphous TNT are transformed into particulate/granular morphology as a result of the solvothermal treatment that confine anatase crystallites preventing further growth during high temperature annealing. A phonon-scattering mechanism at the particle interfaces is proposed to explain the very limited crystallite growth and preservation of the anatase phase. Furthermore, the robust and compact morphology of the nanotubes arrays induced by solvothermal treatment also contributes to its ability to retain tubular architecture at higher temperatures. We also report gas sensitivity and photo-current density of the solvothermally treated anatase TNT annealed at 800 ^oC that show significant enhancement of these properties over the conventional TNT samples annealed at 550 ^oC. The reported work, thus presents an important advancement in the synthesis and structural modification of TiO_2 nanotube arrays, which not only leads to enhancement of properties but also opens up possibilities for high temperature applications.

1. Introduction:

TiO_2 nanotube arrays (TNT) formed by electrochemical anodization of Ti foils are being extensively investigated over the last 10 years because of potential applications in photo-catalysis[1, 2] and photo-voltaics[3, 4, 5, 6] and sensors.[7] In contrast to a network of randomly oriented nanoparticles or polycrystalline thin films, the TNT is supposed to favour unidirectional charge transport along and inside the nanotube walls that may lead to higher charge mobility which is crucial for solar-cell and photo-catalytic performances. However, some recent studies have pointed out that the charge transport rate in TNT is not better than that in nano-particle films[8, 9] because of the presence of exciton-like trap states that limits the performances of TNT based devices at a level lower than that reported for nano-particles film based systems.

The defects and trap states in a TNT system can be reduced by high temperature annealing in oxygen ambience that not only neutralizes the oxygen vacancies but also reduces the grain-boundary related defects (as a consequence of grain growth). On the other hand, the anatase phase of TiO_2, particularly important for its photo-activity, is stable only upto a temperature of around 600 ^oC, beyond a phase transformation from anatase to rutile takes place.[10] Keeping the anatase phase stable at a temperature higher than 600 ^oC with reduced defect densities therefore remains a challenge towards achieving better photo-activity of the TiO_2 based systems. Furthermore, in the case of TNT systems, its far more challenging to retain the tubular morphology and vertical alignment along with maintaining a stable anatase phase at high temperatures. In one of the earlier reports on TNT by Varghese *et al*[11] the nanotube arrays were found to be stable only up to 580 ^oC beyond which a disruption of alignment and orientation was observed. Although the anatase to rutile transformation can be suppressed by extending by extending the transformation temperature above 700 ºC using different metal oxide additives such as Al_2O_3, NiO, SiO_2, ZrO_2, ZnO and Sb_2O_5[12, 13, 14, 15, 16] but this has the disadvantage of forming secondary impurity phases (*e.g.* Al_2TiO_5, $NiTiO_3$) at high temperature. There have been a few reports on the synthesis of pure anatase TiO_2 nanoparticles with high temperature stability[17, 18] however, such a thing has not yet been achieved for TNT. Recently, Lin *et al*[19] achieved high temperature crystallization of free standing anatase TNT and showed their application in the fabrication of DSSC. However, the process involved detachment of the TNT layer from the underlying substrate after anodization and high temperature annealing of the

resulting membrane, followed by attachment of the crystallized membrane onto a glass substrate for device fabrication. In such a process, although the TNT membrane can have high temperature stability, but handling and manipulation of such a free-standing membrane becomes practically difficult on a larger scale. Furthermore, the requirement of attachment to an FTO coated glass substrate may not result in good interfacial properties on a reproducible manner which, in turn, can affect the device performances. A process involving fewer steps that can result in high temperature stability of the anatase TNT is therefore required, which will help in the synthesis of TNT at a larger scale.

We have recently reported that a solvothermal processing of amorphous TNT result in highly crystalline morphology without the disruption of the nanotube architecture.[20] Solvothermal treatment in the presence of iso-butanol at 200 ^{o}C for 2 *h* yields TNT with crystallinity similar to that obtained with conventional (furnace) annealing at 550 ^{o}C. In the present work, we show that such solvothermally treated TNT can be subjected to further high temperature treatment up to 800 ^{o}C with a stable anatase phase along with successful retention of the nanotube architecture having good adhesion with the underlying Ti substrate. Such TNT can not only be useful towards solar cells with lower defects in the light-active material but also serve as substrates for the growth of graphene through CVD process that requires high (800-1000 ^{o}C) temperatures, which can be explored for visible light photo-catalysis. Furthermore, the high temperature stability of TNT will also make them suitable for use in high-temperature gas sensors and in solid-oxide fuel cells. A mechanism for the stability of the anatase phase has been proposed on the basis of phonon-scattering phenomenon at the grain boundaries and its effect on the thermal conductivity of solvothermally treated TNT.

2. Experimental details

Synthesis of TiO_2 nanotubes: Titanium foils (0.25 mm thickness, 99.7% pure, Sigma-Aldrich) were ultrasonically cleaned with deionized water followed by acetone and isopropyl alcohol for 10 min each and dried in nitrogen jet. The anodization was performed in a two-electrode electrochemical cell with the titanium foil as the working electrode (anode) and platinum foil as the counter electrode (cathode) under constant voltage (60V) at room temperature, in ethylene glycol which contains 4 vol% of DIW and 0.2 Wt% of NH_4F. Here the working distance between two electrodes was 3 cm. After completing the anodization process,

TNT film was ultrasonically cleaned in isopropyl alcohol around 15 to 20 seconds to remove debris on the top of TNT.

Solvothermal treatment of amorphous TNT: Solvothermal treatment of TNT was done by placing TNT in 6 ml iso-butanol in Teflon lined autoclave (Parr Instruments, USA) having 23 ml capacity. The tightly closed autoclave was kept in hot air oven at 200^{o}C for 2 hrs, after which it was cooled down to room temperature. The samples were removed from autoclave and were ultrasonically cleaned in isopropyl alcohol around 30 seconds to remove the clogging on the top of TNT. The solvothermally treated TNT samples were subjected to further thermal processing in a conventional high-temperature furnace at different temperatures ranging from 500 ^{o}C to 900 ^{o}C for 2 hrs duration. For comparison, an identical set of samples without the solvothermal treatment (just after anodization, in the amorphous form), were also subjected to similar high temperature furnace annealing.

Characterization: X-ray diffraction (XRD) analysis was performed using a PANalytical X-pert PRO system in glancing angle (2^{o}) mode. The scanning electron microscopy (SEM) was done with the help of FEI Quata 400 system. The high-resolution transmission electron microscopy (HRTEM) was performed with a FEI Tecnai-20-FEG-S-twin system operating at 200 kV. The gas sensing experiments were carried out using an indigenously designed gas sensing set-up, in which, the gas flow was controlled through MKS mass flow controllers and the resistance changes were recorded through an Agilent 4339B High Resistance meter**.** All instruments were interfaced to a computer using LabView® software. Photo-current measurements were done by using CH instruments model 660C electrochemical analyzer using 1M NaOH as the electrolyte, and having the TNT sample and Pt foil as working electrode and counter electrode respectively. A Lumen Dynamics Omnicure S2000 lamp was used to provide UV- Visible illumination in the region 320- 500 nm and the power of 100 mW/cm^2.

3. Results and discussions:

Fig. 1(a) shows the glancing angle XRD patterns of as anodized (AP - TNT) nanotube arrays treated at different temperatures (500-900^{o}C) for 2 h. The corresponding XRD data for solvothermally (iso-butanol) treated nanotubes (IB-TNT) are presented in Fig. 1(b). The identification of the peaks is done after comparing the obtained XRD data was with that of standard anatase and rutile phase data of TiO_2 (JCPDS file no. 894203 and 894920). For

the AP-TNT samples the anatase phase is atable only up to 600 ^{o}C, after which the rutile phase appears and completely dominates in samples treated at 900 ^{o}C. It is also observed that the intensities of all the peaks corresponding to the anatase phase increase with increasing temperature.

Fig. 2(a) shows the Spur–Myers plot for AP-TNT and IB-TNT samples. According to Spur –Myers equation, [21] weight fraction of anatase phase in anatase-rutile mixtures is measured by

$$f = 1 / (1+1.26\, I_R / I_A)$$

Where I_A = integrated intensity of anatase phase and I_R = integrated intensity of rutile phase

In the present case, the value of f is constant up to 900 ^{o}C for IB-TNT samples which reflects the stability of the anatase phase. However, for AP-TNT samples, the value of f starts decreasing from 700 ^{o}C and becomes zero at 900 ^{o}C, which indicates the disappearance of the anatase phase.

To estimate the activation energies of crystallite growth associated with AP-TNT and IB-TNT samples, we use Scott equation[17] that relates the crystallite size with temperature

$$D = C\, exp(-E_a/RT)$$

Where D is the crystallite size obtained from the XRD data (most dominant peak) by using the Scherrer formula; C is a constant; E_a is the activation energy for crystallite growth; R is the universal gas constant and T is the absolute temperature. The plot between ln (D) and ($1/T$) shows a straight line, the slope which gives the activation energy for crystallite growth. Fig. 2(b) presents Scott plots for AP-TNT and IB-TNT samples and the activation energies are found to 16 KJ/mol and 28 KJ/mol respectively. The higher activation energy in IB-TNT samples indicates that the crystallite growth becomes kinetically unfavorable compared to that in AP-TNT samples.

Fig. 3 shows the morphology of AP-TNT and IB-TNT samples through FE-SEM images. Fig. 3(a),(b) and 3(g),(h) shows the top and cross sectional views of AP-TNT (after anodization, amorphous structure) and IB-TNT (after the solvothermal treatment of AP-TNT). It is observed that the as prepared nanotubes have smoother walls and pore mouths (Fig. 3a,b); however, the

solvothermal treatment results in a particulate morphology (IB-TNT, Fig 3g,h). The average size of the nano-particles that constitute the IB-TNT samples, as observed from FE-SEM images, is about 22nm. Fig. 3(c)-(d) and 3(i)-(j) shows the top and cross sectional views of as anodized AP-TNT and IB-TNT after the thermal annealing at 800 ^{o}C for 2 h. It is clear that compared to the AP-TNT samples, the nanotubular morphology of IB-TNT samples are preserved with well defined pore-mouths and cross-sectional structure. Further, when the annealing temperature to 900 ^{o}C the tubular morphology is completely destroyed in AP-TNT (Fig. 3(e)-(f)); whereas for IB-TNT (Fig. 3(k)-(l)), although the pore-mouths are disrupted, but the tubular morphology remains intact. To summarise the FE-SEM observations, we note that the solvothermal processing of TNT arrays helps in preserving the tubular morphology up to about 900 ^{o}C; whereas a single step annealing process of the TNT arrays beyond 800 ^{o}C results in complete destruction of the tubular morphology.

Fig. 4 presents the representative TEM and HRTEM images of the IB-TNT samples before and after annealing at 800^{o}C. As observed from the FESEM images, although the tubular morphology of IB-TNT samples was preserved up to 900 ^{o}C, but disruption of the pore-mouths occurred. Therefore, samples treated at 800 ^{o}C was chosen for a comparative HRTEM analysis to get an understanding of the underlying mechanism for the preservation of the nanotube morphology along with stable anatase phase in solvothermally treated (IB-TNT) samples. Fig. 4(a) shows the TEM picture of IB-TNT and selected area electron diffraction (SAED) shown as the inset. The corresponding high-resolution image is shown in Fig. 4(c). Both the SAED pattern and HRTEM image points to anatase phase *d*-spacing 0.35 nm. Fig. 4(b) shows the TEM picture of IB TNT after annealing at 800 ^{o}C and selected area electron diffraction (SAED) pattern shown as the inset. The corresponding high-resolution image is shown in Fig. 4(d). In this case too, both the SAED pattern and HRTEM image points to anatase phase with *d*-spacing 0.35 nm, thereby confirming the stability of the anatase phase. Furthermore, the HRTEM images reveal that when IB-TNT samples are annealed at 800 ^{o}C (after the solvothermal processing) the average size of the crystallites increase from about 20 nm to only about 30 nm. As we discuss in the next section, the stability of the anatase phase and preservation of nanotube morphology are closely related to the restricted growth of the crystallites that limits the average size to about 30 nm.

It is reported that the stability of the anatase phase of TiO_2 also depends on the crystallite size and the anatase phase is found to be stable with average crystallite size below 30 nm. [17,18] When the as prepared, amorphous (AP-TNT) samples with smoother tube walls undergo a solvothermal processing, a granular or particulate morphology is evolved in the resulting (IB-TNT) samples. Gao and Jelle[22] reported a comparative thermal conductivity study of bulk TiO_2 and the nanotube arrays and found that the thermal conductivity of nanotubes are about an order of magnitude lower than that of bulk powder. They attributed the results to increased phonon scattering and confinement by the nanotube walls. We believe that in the case of IB-TNT samples resulting from solvothermal processing of smooth, amorphous (AP-TNT) nanotubes, the existence of particulate morphology induces further phonon-confinement that results in lowering of thermal conductivity compared to that of AP-TNT samples. Although the individual crystallites within each nano-particle grow under the thermal annealing process, the presence of particle boundaries restricts the crystallite growth beyond 30 nm and hence the anatase phase can be preserved. Furthermore, the solvothermal treatment also results in a very compact nanotube array morphology, that can withstand the thermal stress arising from the underlying Ti substrate and retain the tubular morphology. The higher activation energy obtained from Fig. 2(b) supports the hypothesis that it the growth of the crystallites becomes more kinetically difficult in IB-TNT samples, in which the presence of particle boundaries act as growth inhibitor for the crystallites. Because of the restricted growth of the crystallites to about 30 nm, the anatase phase is retained along with the compact nanotube morphology that also helps in preserving tubular array structure. This is schematically explained in Fig. 5(a) and 5(b).

Fig. 6 shows the Raman spectra of IB-TNT samples. A full scan spectra is shown in the left panel (a) while a high-resolution spectra of the dominant peak is shown on the right panel (b). The anatase phase of TiO_2 has six Raman active modes ($A_{1g} + 2B_{1g} + 3E_g$)[23] appearing at 144 cm^{-1} (E_g), 197 cm^{-1} (E_g), 399 cm^{-1} (B_{1g}), 513 cm^{-1} (A_{1g}), 519cm^{-1} (B_{1g}) and 639 cm^{-1} (E_g). All these modes are observed in Fig. 6(a) and the intensities of these modes increase with increase in annealing temperature. The narrowing of the Raman modes with increase in the intensity indicates enhancement of crystallinity and decrease in the oxygen vacancy defects[24, 25] in the IB-TNT samples. Further, the high-resolution scan of the dominant Raman mode (E_g) at 144 cm^{-1} for samples treated at different annealing temperatures is shown in Fig. 6(b). A clear and distinct shift of this Raman mode (144 cm^{-1}) towards the lower wave number side is observed with

increasing annealing temperature. Such a red shift of the dominant Raman mode with increase in annealing temperature also supports the phonon confinement model as reported in earlier papers.[26]

Fig. 7 shows the methane (CH_4) gas sensing on IB-TNT samples annealed at 800^{o}C, in the form of variation of resistance on exposure to gas as a function of operating (measurement) temperatures and gas concentrations. An excellent repeatability in response to 100 ppm of methane at 200 ^{o}C is observed (shown in Fig. 7(a)). Fig. 7(b) shows the resistance variation at different gas concentrations (100, 500, 1000, 5000 ppm) at 200 ^{o}C. Fig 7(c) and 7(d) shows the comparative sensitivity data at different temperatures and gas concentrations of AP-TNT sample annealed at 550 ^{o}C and that of an IB-TNT sample annealed at 800 ^{o}C. We have also included data for an IB-TNT sample annealed at 550 ^{o}C to compare the effect thermal processing in conventional and solvothermally treated samples. It is to be noted that, for AP-TNT samples, increasing annealing temperature beyond 600 ^{o}C not only induces anatase to rutile phase transformation but also destroys the aligned and vertically oriented nanotube morphology. In both cases (with temperature and gas concentration) highest sensitivity vales are obtained from solvothermally treated IB-TNT sample annealed at 550 ^{o}C. This may be attributed to granular morphology coupled with residual defect states that may help in gas adsorption in IB-TNT (550 ^{o}C) samples. Although, annealing at 800 ^{o}C may reduce the defects in samples compared to that annealed at 550 ^{o}C, the retention of the granular morphology helps in achieving higher sensitivity in IB-TNT (800 ^{o}C) samples compared to that in AP-TNT (550 ^{o}C).

A comparative photocurrent data of AP-TNT (annealed at 550 ^{o}C) and IB-TNT (annealed at 800 ^{o}C) is presented in **Fig. 8.** Photo-current measurements were performed at a constant voltage 0.8 V (vs. Ag/AgCl reference electrode) in 1M NaOH electrolyte. A normalized photo-current of about 2 mA/cm^2 is obtained from IB-TNT at 800 ^{o}C samples compared to about 1.5 mA/cm^2 from AP-TNT at 550 ^{o}C samples. Thus a 33% increase in the photocurrent results from using IB-TNT samples annealed at high temperature of 800 ^{o}C. Such an enhancement of photocurrent not only reflects higher crystallinity but also reduction in the defect density in IB-TNT at 800 ^{o}C samples compared to that in AP-TNT at 550 ^{o}C samples. The photo-current data from an IB-TNT samples annealed at 550 ^{o}C is also included for comparison that shows lower values of current compared to other samples. In this case, scattering losses caused by the

granular morphology and lower crystallinity compared to IB-TNT (800 oC) samples contribute to lower photo-current values.

In conclusion, solvothermal treatment of electrochemically anodized, amorphous TiO_2 nanotube arrays results in a compact and robust architecture with particulate morphology that allows further high temperature stability up to about 800 ^oC, without any disruption to the alignment and vertical orientation. More importantly, the anatase phase of TiO_2 is also preserved, which opens up the possibility for using such array structures as substrates for CNT/graphane growth by CVD process, towards the fabrication visible light responsive nanocomposites. The stability of the anatase phase and retention of the vertically oriented morphology is not possible otherwise, with a conventional annealing of as-prepared amorphous TNT arrays, in which, rutile phase appears along with disruption of the nano-tubular architecture. The FE-SEM and HRTEM images points to the fact that the anatase crystallites are 'locked-in' within the individual particles created by solvothermal process in the walls of the nanotubes that lowers prevents growth of these crystallites during high temperature annealing. In other words, the particulate morphology of the solvothermally treated nanotubes reduces the thermal conductivity by offering higher phonon-scattering at the interfaces, resulting in a very limited growth of the anatase crystallites, thereby preventing anatase to rutile phase transformation. An enhancement of sensitivity to methane gas and about 33% increase in the normalised photo-current density is observed from the solvothermally treated samples annealed at 800 ^oC, compared to that from conventional nanotube samples annealed at 550 ^oC. This is attributed to higher surface roughness and reduced oxygen vacancy defects in such samples. The work opens up the possibility of using solvothermal processing for different metal-oxide nanostructures towards high temperature stability.

Acknowledgement: The financial support from IIT Madras (New Faculty Seed Grant), Department of Science and Technology, Govt. of India (Fast Track Scheme for Young Scientists) and Nissan Research Support Programme is gratefully acknowledged.

References:

1 S. C. Roy, O. K. Varghese, M. Paulose and C. A. Grimes, ASC Nano, 2010, 4, 1259-1278.

2 C. Das, P. Roy, M. Yang, H. Jha and P. Schmuki, Nanoscale, 2011, 3, 3094-3096.

3 K. Zhu, T. B. Vinzant, N. R. Neale and A. J. Frank, Nano Lett., 2007,7,3739–3746.

4 G. K. Mor, S. Kim, M. Paulose, O. K. Varghese, K. Shankar, J. Basham and C. A. Grimes, Nano Lett., 2009,9, 4250–4257.

5 P. Roy, D. Kim, K. Lee, E. Spiecker and P. Schmuki, Nanoscale, 2010, 2, 45–59.

6 D. B. Kuang, J. P. Brillet, C. M. Takata, S. Uchida, H.Miura, K. Sumioka, S. M. Zakeeruddin and M. Gratzel, ACS Nano., 2008, 2,1113-1116 .

7 O. K. Varghese, D. Gong, M. Paulose , K. G. Ong, E. G. Dickey and C. A. Grimes, Adv. Mater., 2003, 15, 624-627.

8 K.N. Zhu, R. Neale, A. Miedaner and A. J. Frank, Nano Lett., 2007, 7, 69-74.

9 C. Richter and C. A. Schmuttenmaer, Nat. Nanotechnol., 2010, 5, 769-772.

10 G. J. Yang, C. J. Li, F. Han and X. C. Huang, J. Vac. Sci. Technol. B., 2004, 22, 2364-2368.

11 O. K. Varghese, D. Gong, M. Paulose , E. C. Dickey and C. A. Grime J. Mater. Res., 2003, 18,156-165.

12 C. N. R. Rao, A. Turner and J. M. Hanig, J. Phys. Chem., 1959, 11, 173-175.

13 K. T. Ranjit, I. Willner, S. H. Bossmann and A. M. Braun, Environ. Sci. Technol., 2001, 35, 1544-1549.

14 D. J. Reidy, J. D. Holmes, C. Nagle and M. A. Morris, J. Mater. Chem., 2005, 15, 3494-3500.

15 K. N. P. Kumar, K. Kiezer and A. Burggraaf, J. Mater. Chem., 1993, 3, 1141-1149.

16 K. V. Baiju , C. P. Sibu, K. Rajesh, P. K. Pillai, P. Mukundan, W. Warrier and K. G. K. Wunderlich, Mater. Chem. Phys., 2005, 90, 123-127.

17 K. Charette, J. Zhu, S. O. Salley, K. Y. Simon Ng and D. Deng, RSC Adv., 2014, 4, 2557-2562.

18 A. L. Castro, M. R. Nunes, A. P. Carvalho, F. M. Costa and M. H. Florencio, Solid State Sciences, 2008, 10, 602-606.

19 J. Lin, M. Guo, C. T. Yip, W. Lu, G. Zhang, X. Liu, L. Zhou, X. Chen and H. Huang, Adv. Funct. Mater., 2013, 23, 5952-5960.

20 B. Manmadha Rao and S. C. Roy, J. Phy. Chem. C., 2014, 118, 1198-1205.

21 R. A. Spurr and H. Myers, Analytical Chemistry, 1957, 29, 760-762.

22 T. Gao and B. P. Jelle, J. Phy. Chem. C., 2013, 117, 1401-1408.

23 T. Oshaka, F. Izumi and Y. Fujiki, Raman spectrum of anatase, TiO_2, J. Raman Spectroscopy, 1978, 7, 321-324.

24 W. F. Zhang, Y. L. He, M. S. Zhang, Z. Yin and Q. Chen, J. Phys. D: Appl. Phys., 2000, 33, 912-916.

25 V. Likodimos, T. Stergiopoulo, P. Falaras, J. Kunze and P. Schmuki, J. Phys. Chem. C., 2008, 112, 12687-12696.

26 P. D. Bersani, X. P. Lottici and Z. Ding, Appl. Phys. Lett., 1998, 72, 73-75.

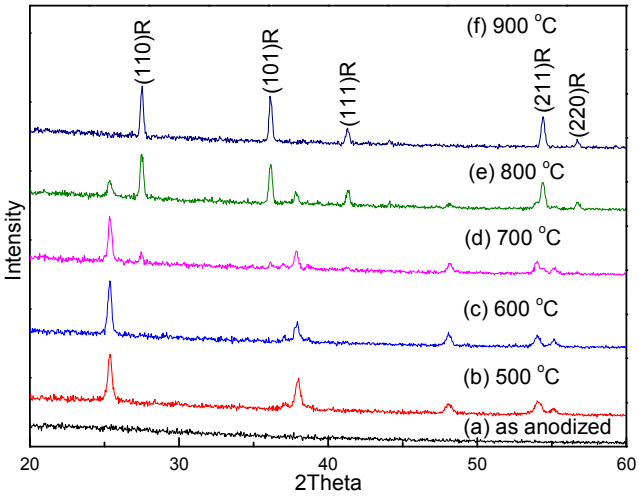

Fig. 1(a) GAXRD pattern of Furnace annealing of AP-TNT

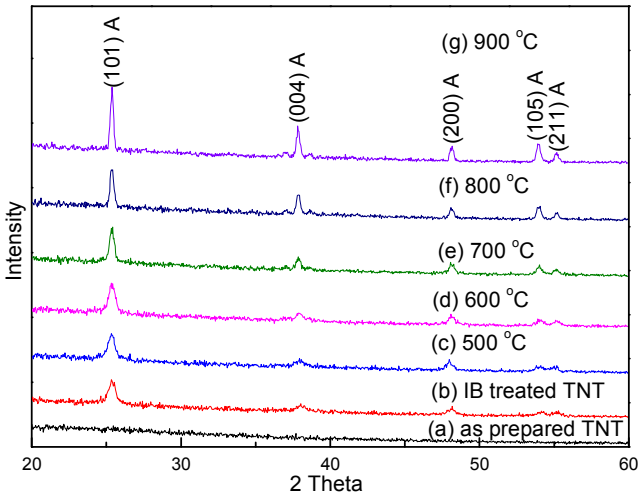

Fig. 1(b) GAXRD pattern of Furnace annealing of IB-TNT

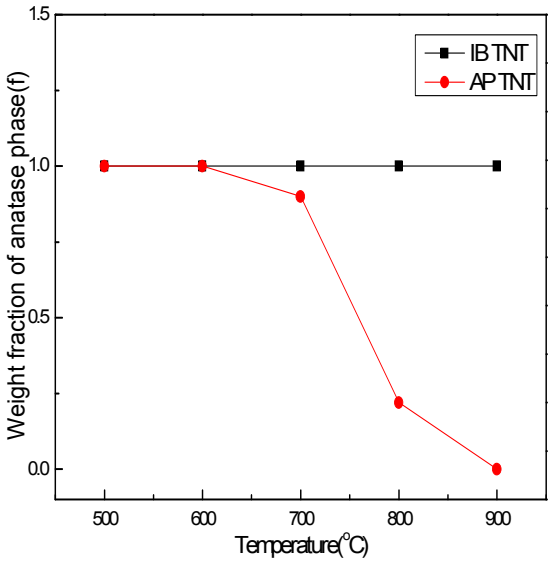

Fig. 2(a) Spur –Myers plot for AP-TNT and IB-TNT

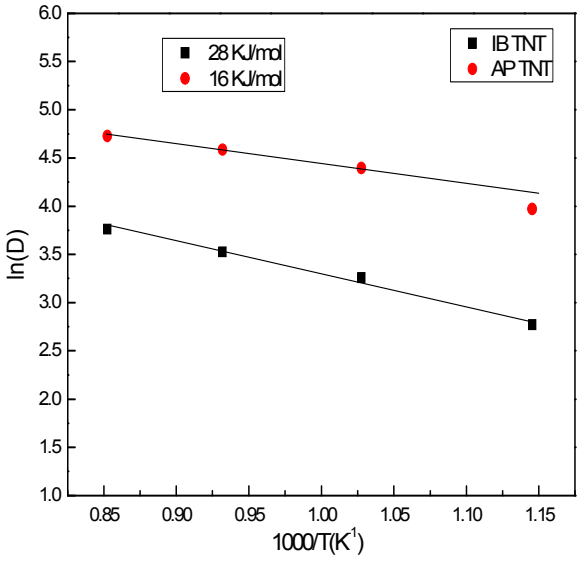

Fig. 2(b) plot of ln(D) Vs 1/T for the equation $D = Cexp(-E_a/RT)$

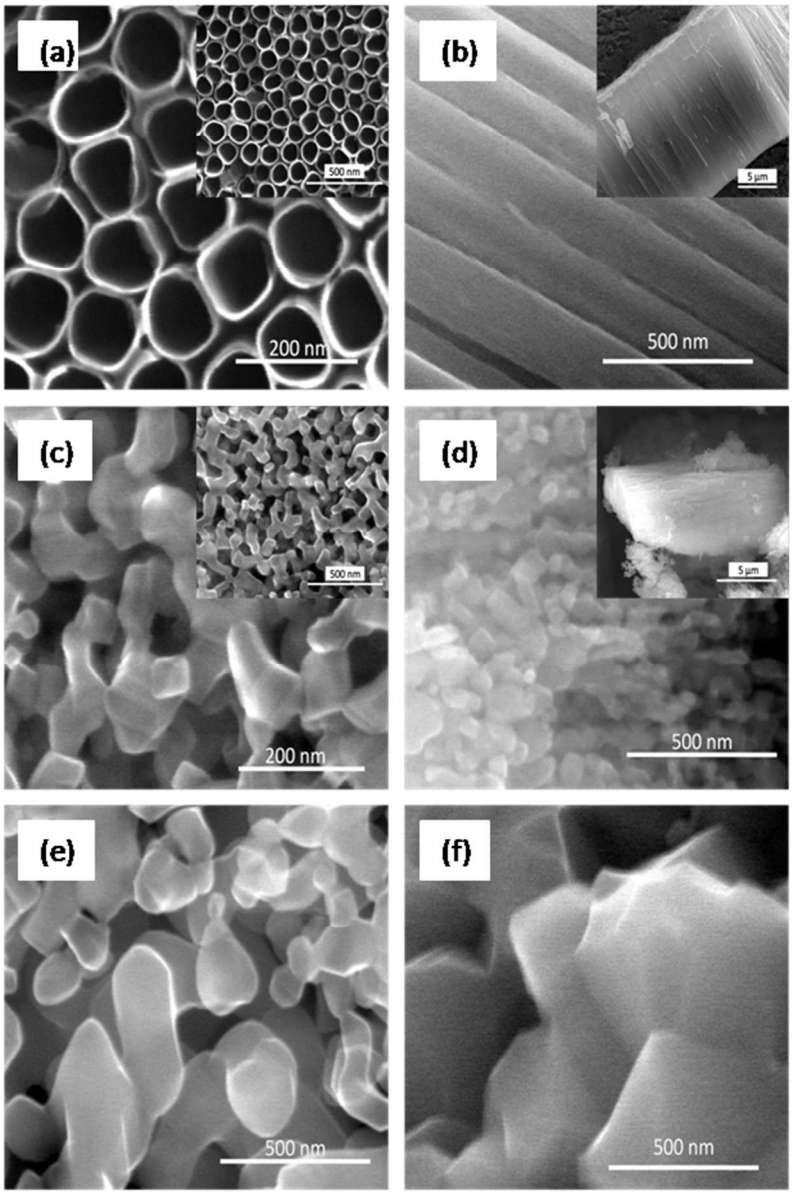

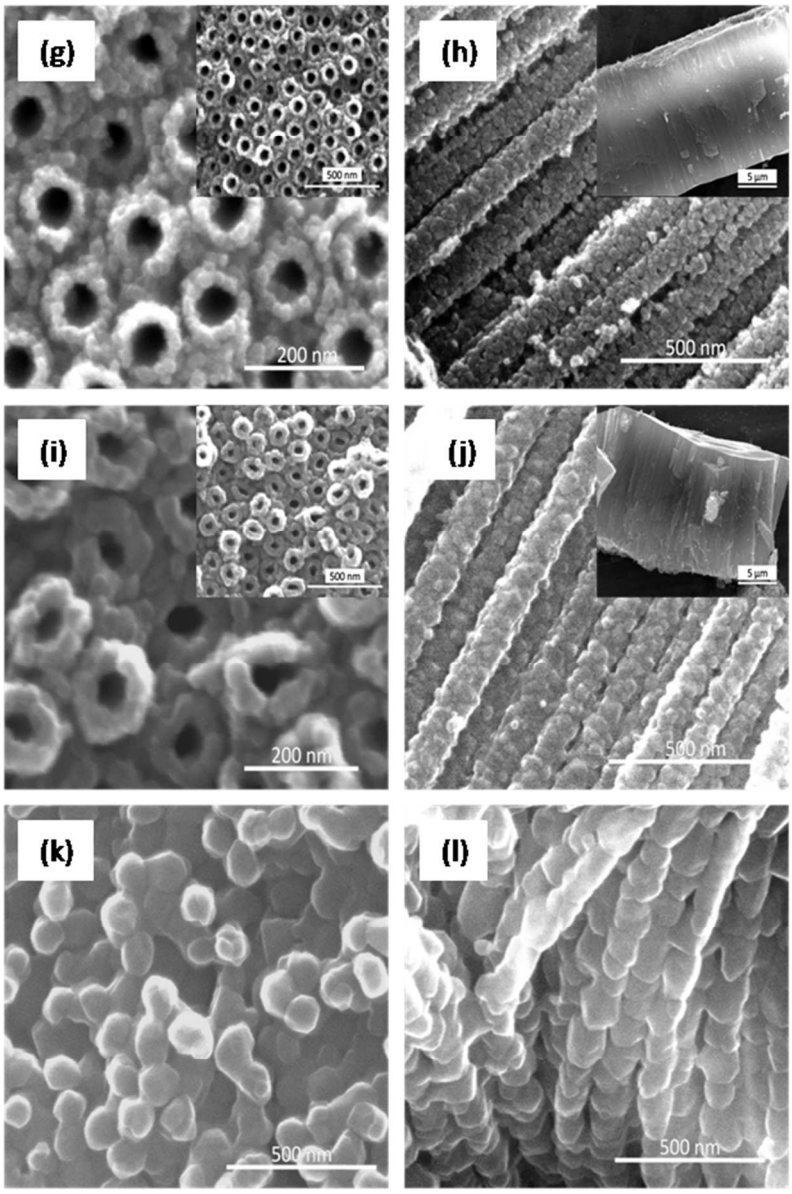

Fig .3(a)-(b) top and cross sectional views of AP-TNT, 3(c)-(d), 2(e)-(f) top and cross sectional views of AP-TNT at 800 ^{o}C and 900 ^{o}C and Fig .3(g)-(h) top and cross sectional views of IB-TNT, 3(i)-(j), 3(k)-(l) top and cross sectional views of IB-TNT at 800 ^{o}C and 900 ^{o}C

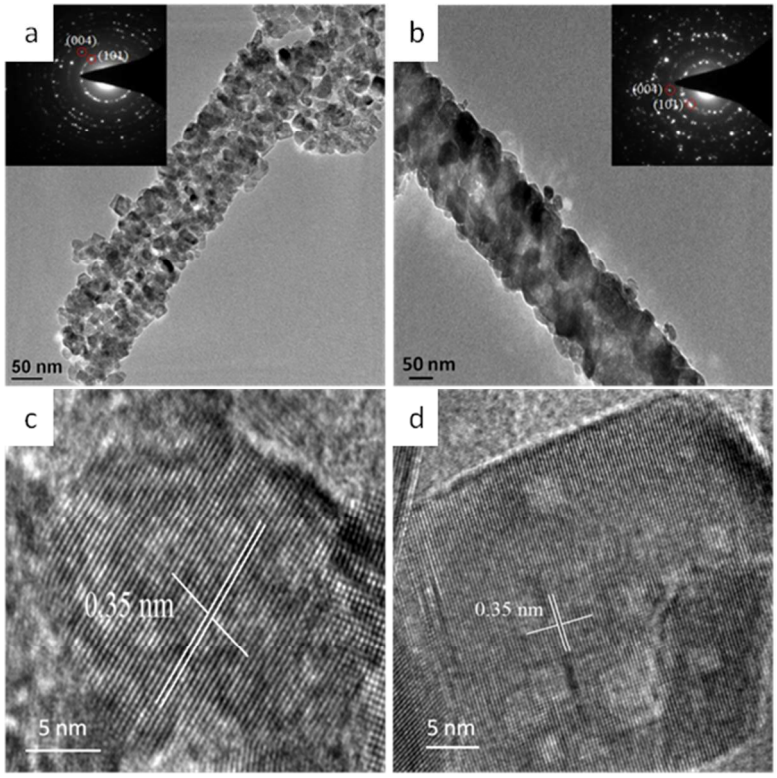

Fig. 4(a),(c) SAED, TEM and HRTEM images of IB- TNT samples and Fig. 4(b),(d) SAED, TEM and HRTEM images of IB-TNT samples after annealing at 800 ^{o}C

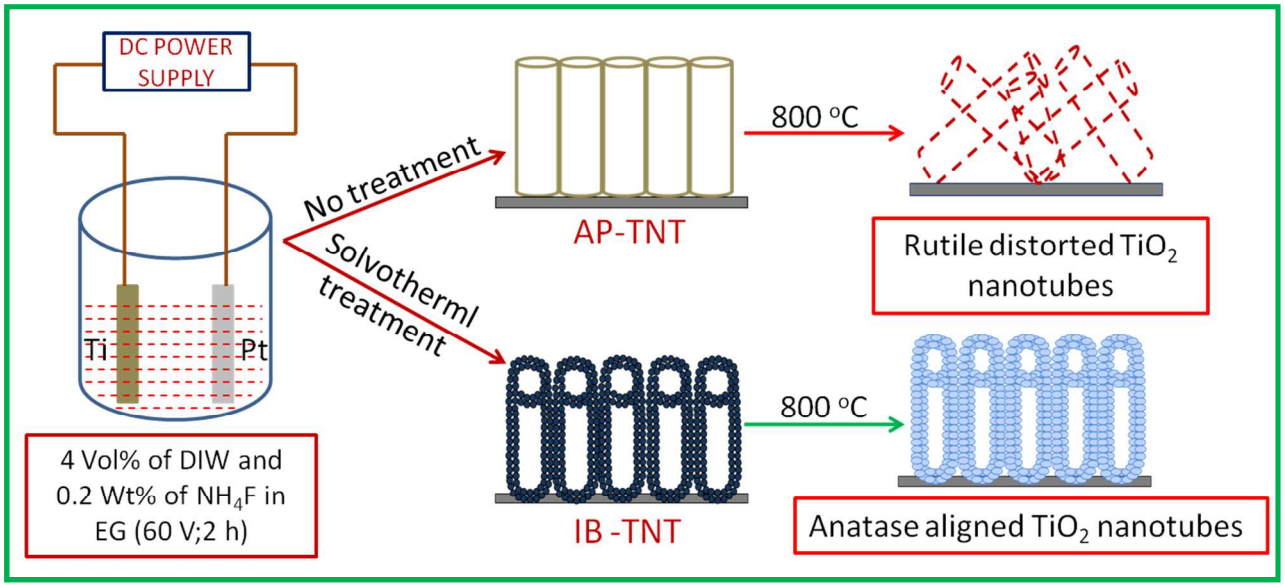

Fig. 5(a) Schematic diagram for annealing processing steps in as prepared TiO_2 nanotubes and solvothermal processed TiO_2 nanotubes in iso-butanol

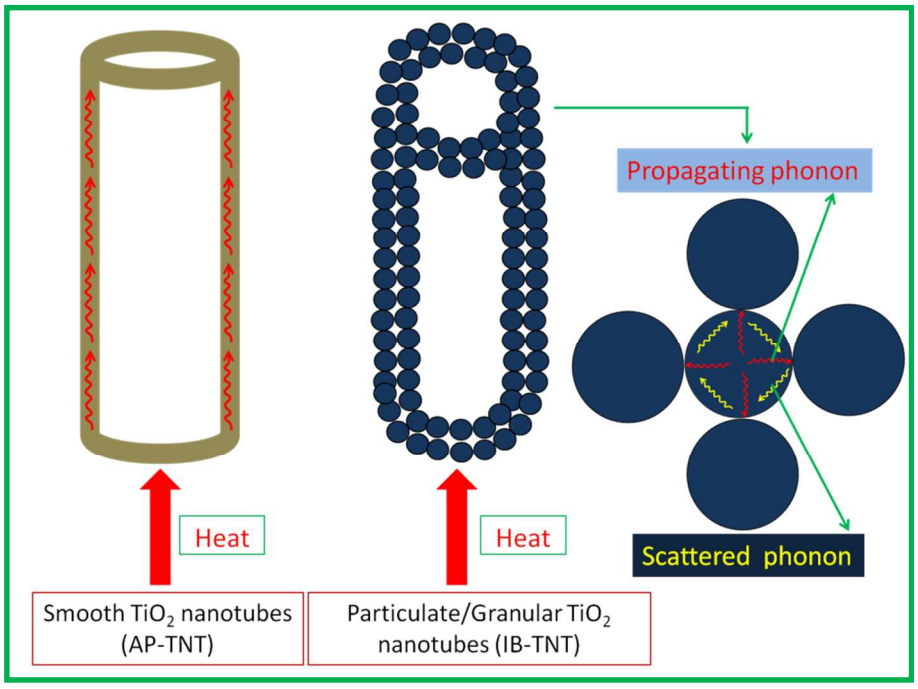

Fig. 5(b) Schematic diagram for phonon propagation in as prepared (AP-TNT) TiO_2 nanotubes and solvothermal processed (IB-TNT) TiO_2 nanotubes

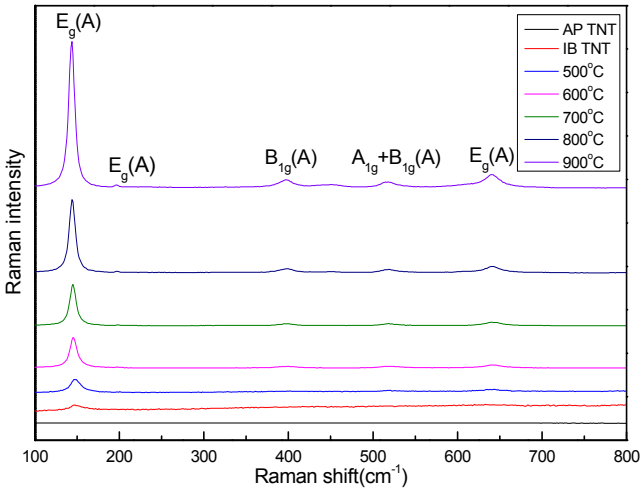

Fig. 6(a) Raman spectra of IB-TNT at different temperatures (500-900 ^{o}C)

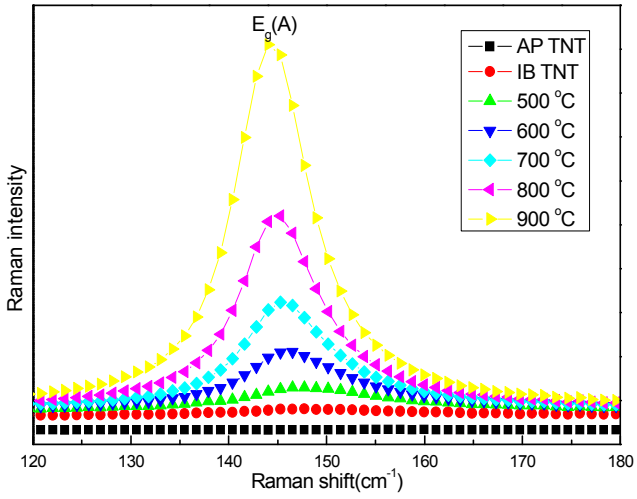

Fig. 6(b) Raman spectra of IB-TNT at different temperatures (500-900 ^{o}C) at144 cm^{-1}

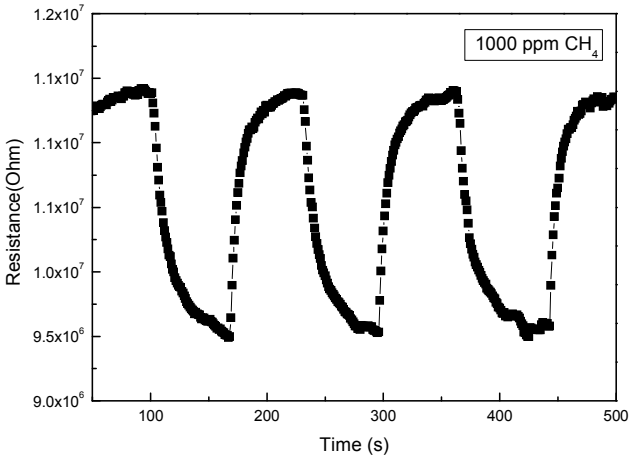

Fig. 7 (a) Repetitive response of the IB-TNT 800 °C to methane (1000 ppm) at 200 °C

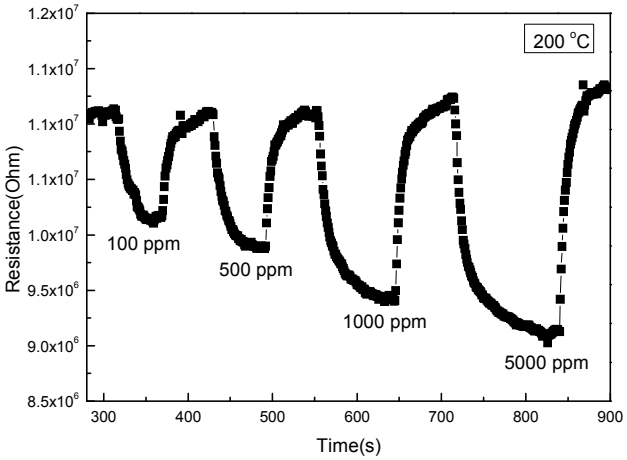

Fig. 7 (b) Response of the IB-TNT at 800 °C to different concentration of methane at 200 °C

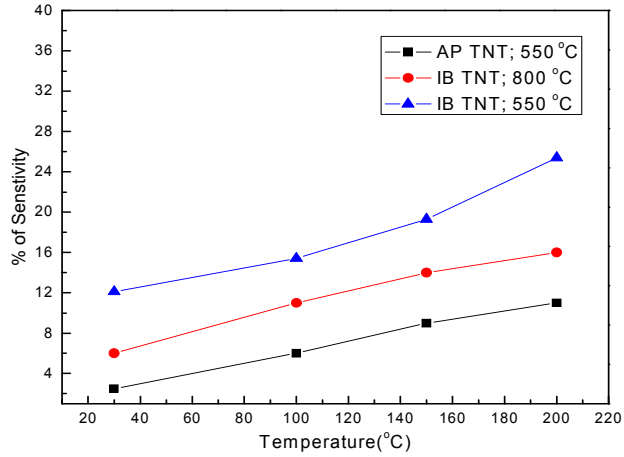

Fig. 7 (c) sensitivity variation with temperature of AP TNT-550 °C, IB TNT-800 °C and IB TNT-550 °C samples

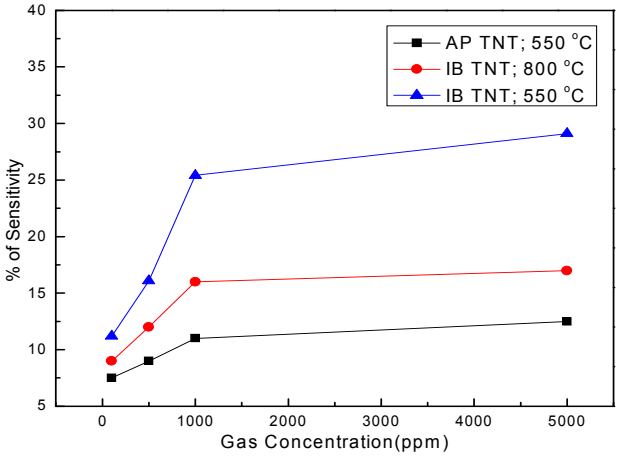

Fig. 7 (d) sensitivity variation with gas concentration of AP TNT-550 °C, IB TNT-800 °C and IB TNT-550 °C samples

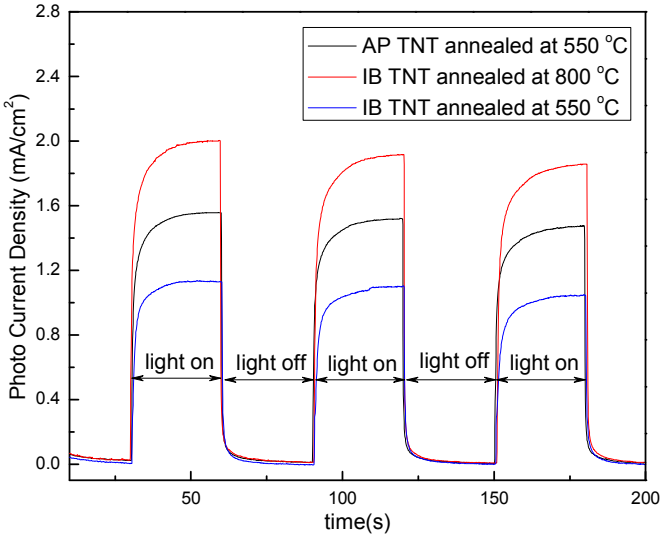

Fig. 8 photo current response of AP TNT-550 °C, IB TNT-800 °C and IB TNT-550 °C samples